A Waddingtonian description of the dynamics of Turing patterns

Shubham Shinde and Archishman Raju*
Simons Centre for the Study of Living Machines
National Centre for Biological Sciences, Tata Institute of Fundamental Research, Bangalore 560065, India
(Dated: June 13, 2025)

Turing patterns are a well-studied model of reaction-diffusion equations for developmental patterning. Their applicability has often been limited by the difficulty in identifying candidate molecules that satisfy the requisite criteria for patterning. Here, we build on recent work on geometric models to describe Turing patterning as a potential flow. We use the mathematics of normal form theory to capture the universal dynamics of Turing patterning, largely independent of the underlying reaction-diffusion equations. We apply our framework to three-component systems and demonstrate that we can accurately capture the dynamics of any given component. We extend our framework to larger networks and to models of Turing patterns coupled with external morphogens that provide positional information. Our normal form equations constitute a quantitative description of the dynamics of chosen markers, and we apply them to the dynamics of SOX9 expression during digit patterning.

I. INTRODUCTION

The Waddington landscape metaphor has been mathematically formalized in recent years in the form of geometric models of cell fate specification [1]. Cell fate data in systems including *C. Elegans* vulval development [2], inner cell mass (ICM) specification in the mouse blastocyst [3] and differentiation of mouse embryonic stem cells (mESC) [4] has been fit to geometric models. These models consider cell fates as attractors in an abstract landscape. The parameters of the landscape are functions of signals that can perturb the fates. The advantage of geometric models is that they are a minimally parameterized description of cell fate data.

However, the original conception of the landscape metaphor was meant to represent developmental trajectories across scales including tissues and entire phenotypes [5]. The application of the Waddington landscape to multi-cellular systems undergoing spatial patterning is less clear although it has been explored in some contexts [1, 6–8]. Here, we study how Turing patterns can be described by such a landscape.

Turing patterns are one of the oldest models for spatial pattern formation in the context of developmental biology [9]. The most well-known mechanism of Turing patterns is the activator-inhibitor system [10]. Despite some success in identifying candidate activator inhibitor pairs [11–13], it has generally been difficult in developmental systems to identify candidate molecules whose regulatory connections and diffusivities satisfy the requisite criteria for Turing patterns [14–16].

The proposal that a three-component Bmp-Sox9-Wnt network could be responsible for the patterning of digits in mice has therefore excited considerable interest in the investigation of Turing patterns with three or more components, some of which may be non-diffusible [15, 17, 18]. Further, it has been suggested that the coupling of Turing patterns with other morphogen gradients can lead to more complex dynamics [19–21].

These models are all described by reaction-diffusion equations. The reaction terms are typically phenomenological with different models making different choices. Parameter values like rate coefficients, thresholds etc. are rarely known and the complexity of signaling pathways is typically not modeled.

It is therefore useful to describe Turing patterning from a geometric point of view. The usual approach in modeling Turing patterns is to identify relevant molecular constituents, and describe their dynamics with a set of reaction-diffusion equations. The linear stability analysis of these equations is usually simple and a substantial amount of work has been done over the years to understand their nonlinear dynamics. For example, it is common to apply a perturbation theory in the bifurcation parameter, which gives rise to the so-called amplitude equations [22–25]. These equations can be used to approximate the nonlinear dynamics of any given set of reaction-diffusion equations near a bifurcation.

In practice, one may observe the concentration of a localized patch of one or more component molecules (e.g. morphogens) increase in time and saturate without full knowledge of all relevant regulatory components. In this work, we instead ask what is the minimally parameterized way to describe the dynamics of such a putative Turing pattern. We do this by simplifying the dynamics of Turing patterns for arbitrary reaction-diffusion equations using the mathematics of normal form theory. In doing so, we find the terms that one should write down *apriori* that will describe the dynamics of the concentration of a given component. This allows us to describe Turing patterns as the motion of emergent variables on a landscape and identify the universal parameters that govern their dynamics.

We show the utility of our method by comparing our geometric approximation to numerical solutions of various three and more component Turing networks. We

* archishman@ncbs.res.in

also extend our framework to include Turing networks where a parameter is dependent on a spatially varying morphogen profile. Finally, we apply our framework to study the dynamics of SOX9 expression in the context of digit patterning.

II. RESULTS

A. Normal form theory gives a low-dimensional description of reaction-diffusion equations

Turing patterns are modeled as reaction-diffusion equations. We assume that these equations can be written in the following general form

$$\partial_t \boldsymbol{u} = \boldsymbol{f}(\boldsymbol{u}) + D\nabla^2 \boldsymbol{u}, \tag{1}$$

where $\boldsymbol{u} = [u_1, u_2, \cdots]$ are the components of the network whose values are the concentrations of component molecules (e.g. gene expression), D is a diagonal matrix with diffusion constants (some of which could be zero), $\boldsymbol{f}(\boldsymbol{u})$ are reaction terms which are nonlinear in general and reflect regulatory and signaling interactions between underlying components, and ∇^2 is the Laplacian. Since we are interested in localized patterns, we use periodic boundary condition unless mentioned otherwise. The Turing instability is diffusion-driven. We assume the reaction terms are stable around a homogeneous state $\boldsymbol{u}_0$ given by $\boldsymbol{f}(\boldsymbol{u}_0) = \boldsymbol{0}$. Around this homogeneous state, the equations can be linearized. The Fourier modes are a natural coordinate system and, typically, the homogeneous state is unstable to only a few modes. A small perturbation around the homogeneous state evolves into a patterned state in the components but typically only a few components are measured (Fig. 1). As we show below, the normal form of the dynamics of these modes can be seen as motion on a potential landscape. Attractors on the landscape correspond to stable patterned states. Biological perturbations to the underlying network, like a mutant corresponding to the deletion of a node, can lead to a different observed pattern (Fig. 1). Changes in molecular interactions are captured by changes in the effective parameters of the landscape which can tilt the landscape so the dynamics goes to a different attractor. We demonstrate how to systematically recover the observable expression from the coordinates of the landscape. Hence, the landscape is a useful and universal parameterization of the dynamics independent of the details of the underlying networks of interactions.

To derive the normal form of the dynamics, we assume that there is only one eigenvector in component space that has a potential instability, which is typical of diffusion-driven instabilities. In this case, it suffices to consider a scalar equation for the amplitude of the Fourier modes of the eigenvector. The nonlinearity in Equation (1) can be Taylor expanded to give the equations of motion in Fourier space. The form of these equations can be deduced from symmetry arguments [26]. The idea behind normal form theory is to simplify the equations by analytic change of coordinates [27], which perturbatively eliminates nonlinear terms based on their degree in the polynomial expansion. To any polynomial order, nonlinear terms can be removed by a change of coordinates except for the so-called resonant terms (Section II, SI). The linear terms determine the extent to which the equations can be simplified.

We find the normal form of the equations near the Turing bifurcation. For a single Fourier unstable mode k, the equation for the amplitude of the unstable mode in its normal form ($\tilde{z}_k$) is given by

$$\dot{\tilde{z}}_k = \lambda_k \tilde{z}_1 - \beta_3 \tilde{z}_k |\tilde{z}_k|^2, \tag{2}$$

where λ_k and β_3 are parameters to be fit from the data. All the terms of order higher than five can be eliminated in the normal form equation and we do not require the fifth order term in practice (Section II B, SI). Intuitively, the normal form equations capture the essential nature of the dynamics near the unstable fixed point. Any corrections to the dynamics are given by coordinate changes.

This is shown in Fig. 2 where r_1 and r_2 correspond to the radial components of the complex amplitudes of an unstable mode (z_1) and a stable mode (z_2). In the original coordinates (Fig. 2A), the homogeneous state is unstable (at $r_1 = r_2 = 0$) and the stable patterned state has a contribution from both modes. In the normal form coordinates (Fig. 2B), the dynamics is simplified to lie only along one of the coordinates ($\tilde{r}_1$). Given data on the concentration of a molecular component, we can project it onto the normal form coordinate and fit a universal form to the dynamics (Fig. 2B). Along with the dynamics of the normal form coordinate, we can also fit a time-independent coordinate change that captures the dependence of all other modes on the dynamics of a *single mode*. As shown below, we can predict the general form of these coordinate changes using a perturbation theory.

B. The spatio-temporal dynamics of Turing patterns is captured by normal form dynamics with corrections from coordinate change

Here, we develop how coordinate changes can be done in a systematic way to approximate the dynamics of any given equation. To relate the dynamics in the normal form coordinates to the concentration of a molecule, we need a map from the normal form coordinates to the observable expression. This map is obtained by coordinate changes.

In general, the coordinate changes involve all of the modes. However, we assume that the dominant contribution to the coordinate changes comes from the unstable modes. By considering all terms allowed by symmetry in the equations for the stable modes (Section I, SI), and keeping only the ones which involve the unstable modes, we obtain a map for the stable modes (Methods). If there

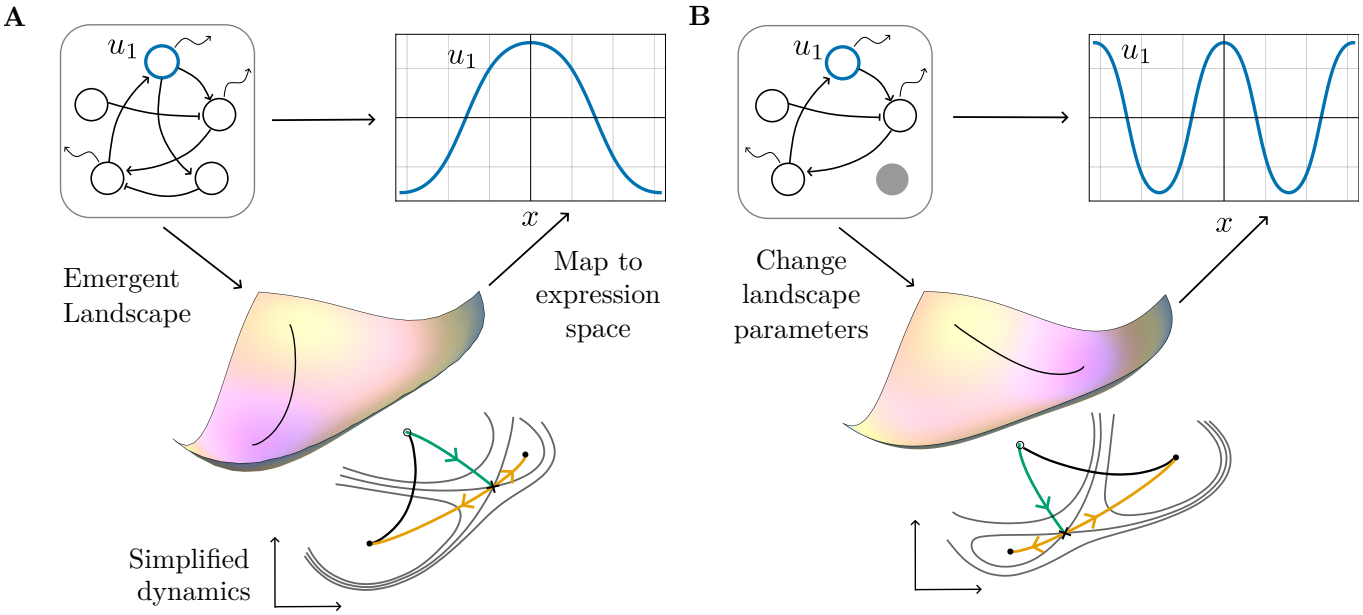

FIG. 1. **The dynamics of Turing patterns has an emergent landscape description.** (A) Turing patterns are described by reaction-diffusion equations for a set of components that regulate each other's activity (diffusible components are shown using wiggly arrows in the network). These components could be signaling ligands, transcription factors (TFs) etc. The activity of any given component (u_1 in this case) makes a pattern. As we show in the text, the dynamics of the activity of any given component can be thought of as motion on a landscape. Minima of the landscape correspond to entire patterned state. The dynamics on the landscape has a form which is often simple and independent of the details of the underlying regulatory network. A time-independent map from the landscape to the expression of u_1 allows us to quantitatively capture the dynamics of u_1. (B) Biological perturbations like mutants (e.g. deleting a node) or changes to signaling can change the trajectory and lead to a different pattered state. The perturbations can be parameterized in the landscape, resulting in a tilted landscape which takes the same initial point to a pattern with two bumps. The streamplots show changes in the basins of attraction for the pattern with one and two bumps.

is only one unstable mode, ($k = 1$), then for $k \geq 2$ we get

$$z_k = \frac{\beta_k \tilde{z}_1^k}{k\lambda_1 - \lambda_k}, \tag{3}$$

where β_k are undetermined coefficients and λ_k are the stable eigenvalues. The coordinate transformation is time-independent. For a single unstable mode, the dynamics of the concentration of any molecule $u(x,t)$ is thus given by

$$u(x,t) = u_0 + \tilde{z}_1(t)e^{ix} + \sum_{k\geq 2} \frac{\beta_k}{k\lambda_1 - \lambda_k}\left[\tilde{z}_1(t)e^{ix}\right]^k + \text{c.c.} \tag{4}$$

Note that this form is independent of the underlying equations. It depends only on the form of the dispersion relation λ_k and parameters β_k which are to be determined by a fit. We now show that a small number of modes are able to capture the dynamics of Turing patterns very accurately.

To test our results, we use a three-component Turing network with one non-diffusible component (Methods). The network is modeled after the Bmp-Sox9-Wnt network in Ref. [28] but we use Hill functions instead of cubic nonlinearities to model interactions between components. The network structure is shown in Fig. 3A. One of the components (u_3) is non-diffusible which leads to a saturation of the dispersion relation at large wavenumber (Section III A, SI).

For the case of a single unstable mode ($k = 1$), we first fit the dynamics of the mode to the normal form equation (Fig. 3B). The dynamics of the normal form coordinate with periodic boundary conditions is shown in Fig. 3C. The state with homogeneous concentration is an unstable fixed point. The dynamics goes along the unstable direction towards a circle of fixed points and the angle corresponds to the positioning of the center of the single bump. We use the form in Equation (4) keeping only a few modes and fitting to the undetermined parameters (Methods). We show the numerical solution along with our fit in Fig. 3B. The case of two unstable modes ($k = 1, 2$) can be studied similarly (Methods). The unstable manifold now has two unstable modes, and we can first fit to their dynamics (Fig. 3D). The dynamics is shown in the radial coordinates of the two unstable modes which, along with our normal form fit, is shown in Fig. 3E. Our normal form approach is therefore able to capture fairly complex spatio-temporal dynamics.

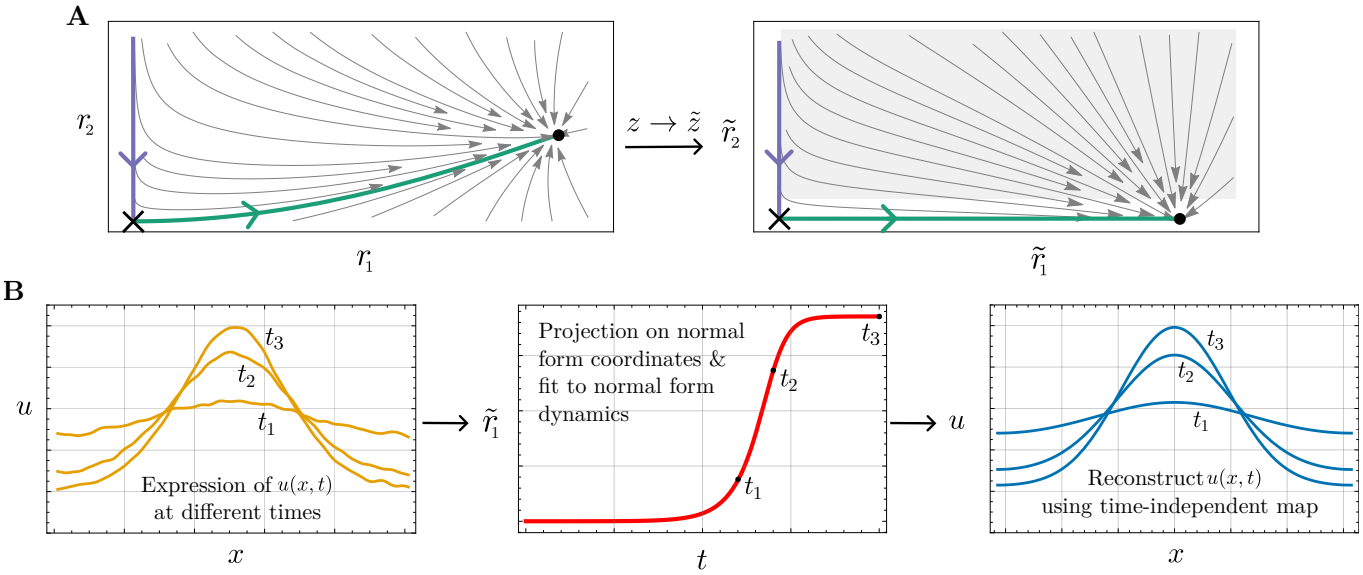

FIG. 2. **Parameterization of Turing patterns by normal form dynamics with corrections from stable modes.** (A) Fourier modes serve as a natural basis for the dynamics of components in models of Turing patterns. Here we show plot of the radial part of the dynamics of one unstable (z_1) and one stable (z_2) mode. The initial state ($r_1 = r_2 = 0$ denoted by cross) is unstable and the dynamics goes to a patterned state which generically has both modes (denoted by the filled circle). Upon change of coordinates, we get the normal form for the dynamics where the dynamics of the unstable mode is decoupled and hence, the unstable manifold is along the first normal form coordinate ($\tilde{r}_1$). In the normal form coordinates, we can ignore the dynamics of the stable mode (shaded gray) and the problem becomes effectively low dimensional. (B) Given spatio-temporal data for the component of interest, we project it onto the normal form coordinates and fit to the normal form dynamics given by Equation (2). As the dynamics of the original Fourier modes can be written entirely as a time-independent function of the normal form coordinate, we can reconstruct the dynamics of the component of interest using just the normal form dynamics and the time-independent map.

C. Patterns on 2D domain are complex and require more eigenfunctions to describe the dynamics

In two dimensions, the plane wave $e^{i\boldsymbol{k}.\boldsymbol{r}}$ is an eigenfunction of the Laplacian $\nabla^2 = \partial_x^2 + \partial_y^2$ with eigenvalue $-(k_x^2 + k_y^2) = |\boldsymbol{k}|^2$ and positional coordinate $\boldsymbol{r}$. Thus the growth rate depends only on the absolute value of the wavevector $\boldsymbol{k}$. As a result, in two dimensions, there will be many combinations of k_x and k_y that are unstable. Nevertheless, these will be discrete on a bounded domain. This allows us to use our formalism for two-dimensional patterns, which we do on a square domain. We now get one equation for each k_x and k_y mode which is unstable (Methods). The solution $u(x, y, t)$ is a superposition of all the allowed modes and corrections to stable modes are included as before. As an example, we show a stripe pattern in Fig. 4A. In this case, we can ignore the k_y mode as the instability is along the x direction. To simplify things further, we only examine the dynamics of the central stripe by restricting our attention to its neighborhood. When projected along the y axis, the dynamics is captured well by our normal form equations (Fig. 4B). Further, the spatial pattern is now distinctly composed of several modes, but including a small number of modes again suffices to give a very good approximation to the full spatio-temporal dynamics (Fig. 4C).

D. Patterning dynamics for large networks can be captured with the same parameterization

The real strength of our formulation is revealed in a consideration of more complex networks. Contrary to the simple networks discussed previously, regulatory and signaling networks are generally complex and involve many interacting components. Even with the addition of more components in the network, the essential structure of the dynamics remains unchanged. Our normal form coordinates capture this essential feature, making it largely independent of the specific details of the individual components. To demonstrate this, we analyze a network with ten components and approximate it with our normal form dynamics.

As the number of components increases, identifying parameters that lead to Turing patterns becomes increasingly difficult [17]. We construct our network (Fig. 4D) by assuming the Jacobian is a random matrix whose eigenvalues are all negative, ensuring the stability of the homogeneous state [29, 30]. We then search for diffusion constants that give a few unstable modes (Section III B, SI). We assume that only a few components are diffusible. To saturate the dynamics, we add cubic terms to the equations. For one unstable mode, the projection of the numerical solution along the unstable mode can be fit

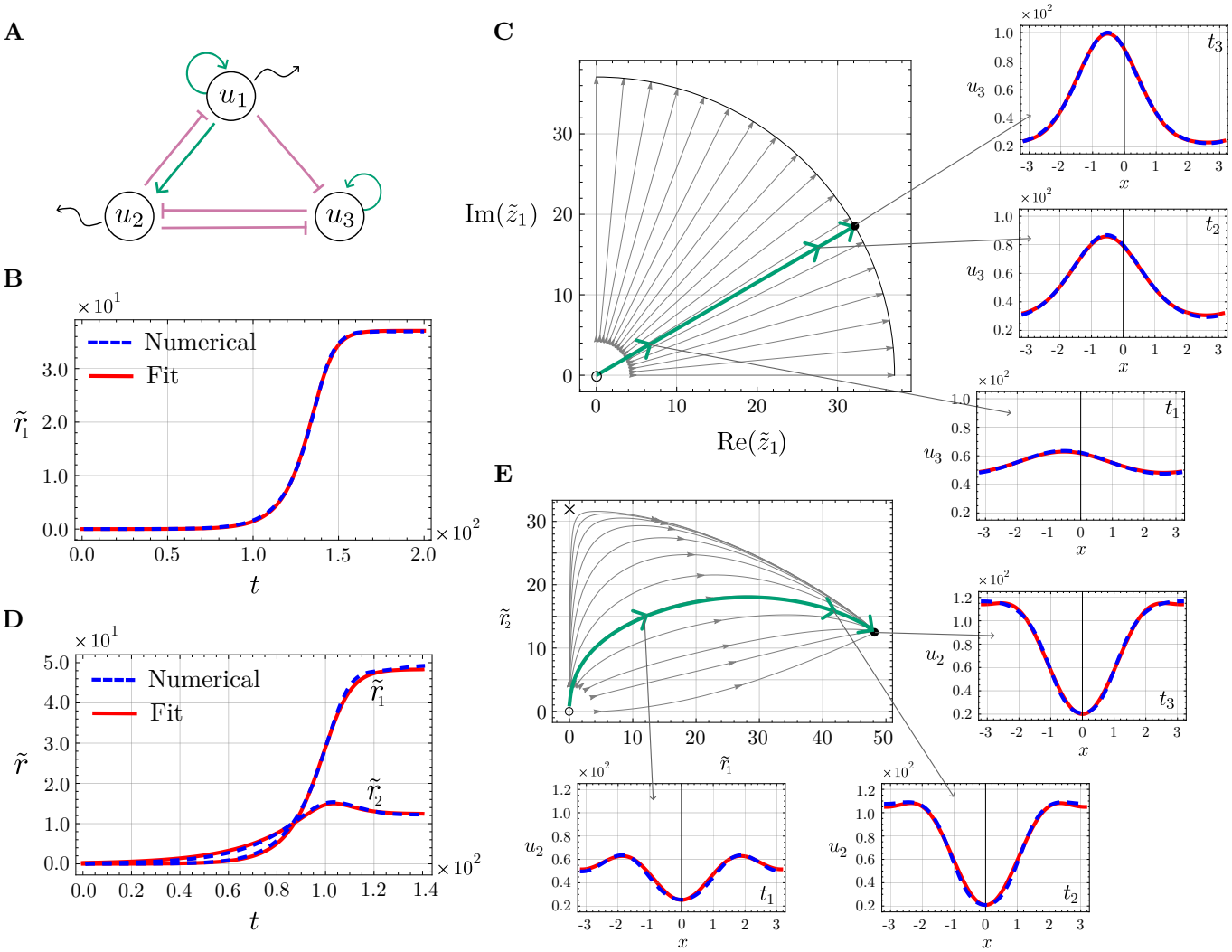

FIG. 3. **Normal form captures the dynamics of three-component Turing networks.** (A) A 3-component network with a non-diffusible component u_3, with activatory (green) and inhibitory (purple) links. (B) Projection of the numerical solution of $u_3(x,t)$ obtained by solving the reaction-diffusion equations on the unstable mode (blue, dashed) and fit (red) to the radial part of $\tilde{z}_1$ dynamics. (C) The flow of $\tilde{z}_1$ dynamics. Small perturbations away from the origin (homogeneous state) grow radially and stabilize on a ring of fixed points. The angle determines the position of the bump and remains constant. Only one quadrant is shown. The normal form approximation (red) is shown alongside the numerical solution of u_3 (blue, dashed) at time $t_1 = 120, t_2 = 140$, and $t_3 = 200$. (D) For two unstable modes, the projection of u_2 dynamics along the unstable modes (blue, dashed) and normal form approximation (red) of the radial part of the dynamics of $(\tilde{z}_1, \tilde{z}_2)$. (E) We show the radial flow of the two unstable modes going to a final patterned state. The numerical solution of $u_2(x,t)$ (blue, dashed) along with the normal form approximation (red) is shown at $t_1 = 90, t_2 = 110$, and $t_3 = 130$.

with the universal normal form equation (Fig. 4E). Despite the complexity of the network, our normal form approximation fits the dynamics well. The fit for a diffusible (u_2) and a non-diffusible (u_8) component of the network at different times is shown in Fig. 4F.

E. Coupling positional information with Turing patterns gives reproducible patterns

Recent proposals suggest that Turing patterns can be coupled with positional information to give spatial patterns that may be more robust and reproducible [19, 31]. We extend our framework to the case of guided pattern formation by coupling Turing patterns to other morphogens.

The resulting dynamics from the coupling of the two mechanisms can be classified depending on whether the

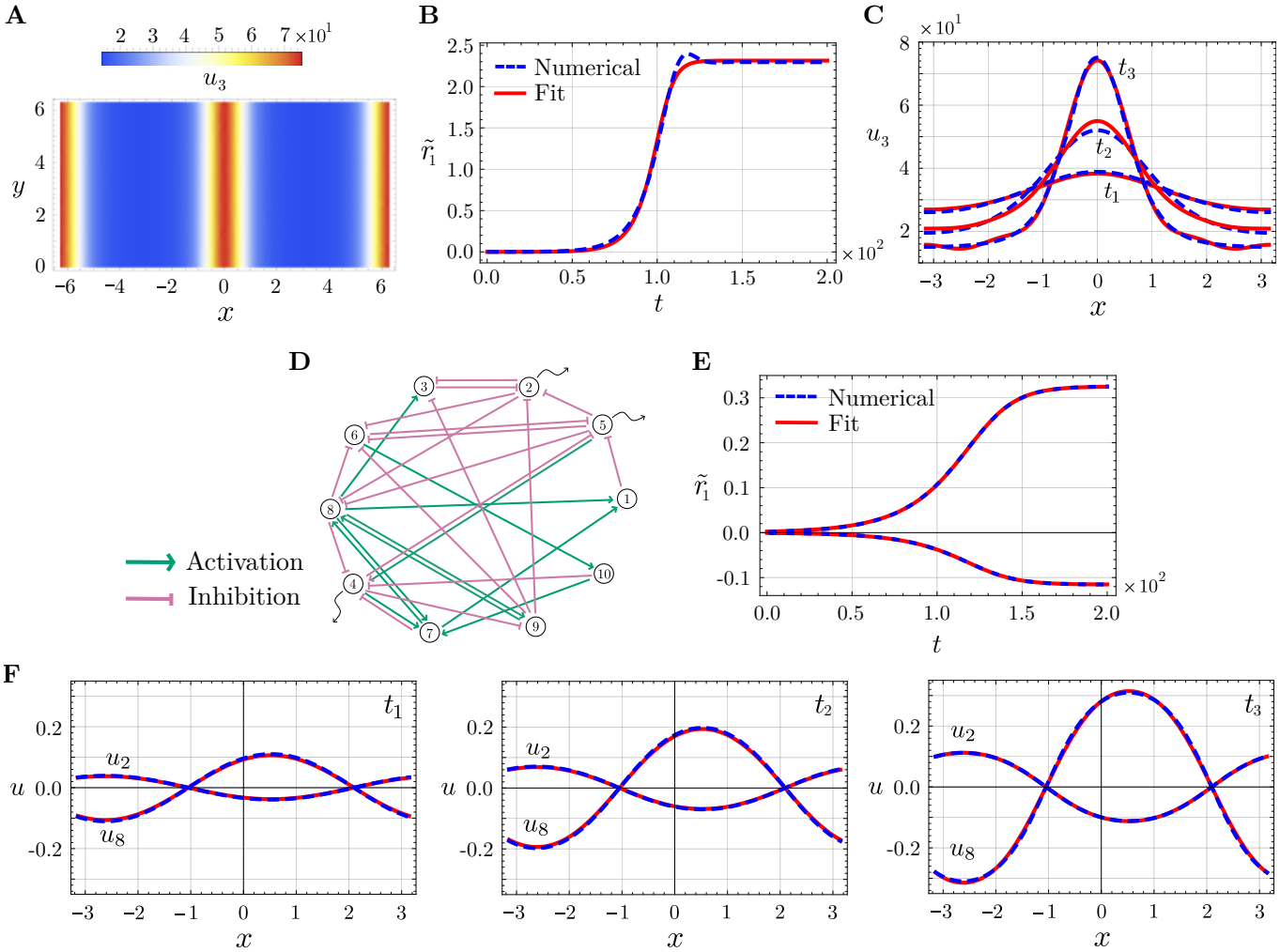

FIG. 4. **Generalization to patterns on 2D spatial domain and large networks.** (A) Numerical solution of the dynamics of $u_3(x, y, t)$ on 2D spatial domain. (B) Projection of the numerical solution of the central stripe along the unstable mode (dotted blue) and fit (red) to the radial part of the dynamics of $\tilde{z}_1$. (C) Spatio-temporal dynamics of the central stripe (blue, dashed) with fit (red) to normal form dynamics with corrections from 3 stable modes at time $t_1 = 90, t_2 = 120, t_3 = 150$. (D) A random network with 10 components which are activating or inhibiting. Diffusible components are shown with wiggly arrows. (E) The dynamics of the radial part of the projection of the numerical solution of u_2 and u_8 components along the unstable mode (blue, dashed) along with the normal form approximation (red). (F) Spatio-temporal dynamics of a diffusible component u_2 and non-diffusible component u_8 (blue, dashed) and fit (red) to normal form dynamics with corrections from one stable mode at time $t_1 = 100, t_2 = 120$, and $t_3 = 200$.

spatial eigenfunctions are perturbed. For simplicity, we consider the dynamics in one spatial dimension. The general form of the equations now becomes

$$\partial_t \boldsymbol{u} = \boldsymbol{f}(\boldsymbol{u}, x) + D\nabla^2 \boldsymbol{u} + \boldsymbol{h}(x), \tag{5}$$

where the reaction terms $\boldsymbol{f}$, can now explicitly be dependent on x and $\boldsymbol{h}(x)$ is a production gradient. The production term $\boldsymbol{h}$ leads to an inhomogeneous unstable fixed point but does not change the eigenfunctions around the fixed point. It also breaks translational symmetry and we have only one stable point in $\tilde{z}_1$ plane (Fig. 5A). For small perturbations, the dynamics evolves quickly along the radial direction with a constant angle, and then evolves along the angular direction with constant radius (Fig. 5A). Thus, the evolution along the radial and angular directions can be separated. This corresponds to the growth of the pattern followed by a translation to align the peak (Fig. 5A). In this manner, the production gradient can align the pattern along a particular axis. The evolution along the angular direction can be approximated to $\dot{\theta} = -pr_0^{-1}\sin(\theta)$, where p is the projection of the production gradient along the first mode and r_0 is the radius of the ring (Methods). The radial dynamics requires two parameters to fit as before and the angular dynamics requires one additional parameter (Methods). The fit of our normal form approximation to

the dynamics of the pattern at different times is shown in Fig. 5A.

A more complex case is given by a wavefront of morphogen traveling at some velocity v, which modulates reaction term $\boldsymbol{f}$ in Equation (5). This leads to the sequential appearance of patterns. Interestingly, SOX9 expression along the anterior-posterior (AP) axis during limb bud development shows such a sequential appearance [28]. Pattern formation on an apically growing domain also gives similar sequential dynamics [32, 33]. As the domain grows, there is more area for the pattern to form. Hence, modulating a parameter via a front and apical domain growth are mathematically similar [32].

We approximate the wavefront by changing it in discrete steps and assume that the morphogen modulates a parameter to take the system from a non-patterning to a patterning region (Fig. 5B). A bump develops locally initially followed by the development of another peak in an adjacent sub-domain. Essentially, each bump grows independently except at the boundary, where continuity requires that their dynamics be connected. The eigenfunctions for a fixed morphogen pattern can be calculated numerically and are localized.

We therefore obtain an 'independent bump' approximation, and the pattern as a whole can be written as a sum over localized eigenfunctions. We can fit this to the first two bumps and again obtain simple growth governed by our previous normal form equation (Fig. 5D). If the patterning dynamics is very slow compared to the speed of the morphogen, the two curves in Fig. 5C come closer to each other and eventually collapse giving back Turing patterning with a single effective mode (Section III D, SI). We use our eigenfunctions to fit the data for SOX9 expression in Ref. [28] along the AP axis for three different time points. The fit shown in Fig. 5F is suggestive that this simple approximation may be able to quantitatively capture this data. The comparison of the profile of our fit to the data is shown in Fig. S5 in the SI.

III. DISCUSSION

Turing patterns have received extensive theoretical attention over the years as a model for developmental pattern formation. However, their applicability has been somewhat limited due to the lack of suitable molecular candidates which can implement the proposed mechanisms. Here, we show that there are certain universal features of Turing patterns independent of any particular dynamical implementation. We discover these by writing the 'normal form' of Turing pattern formation. In doing so, we find that Turing pattern formation can be written as a potential flow, akin to Waddington's landscape. While in simple cases the equations are directly in the form of a potential flow, more complex cases may require a metric to write in potential form [1].

The coordinates of the landscape, which are usually seen as abstract, are clearly defined in our framework. They correspond to Fourier modes and can be derived in a very general way as we demonstrate. The stable fixed points correspond not to cell fates, but a particular pattern over many cells. Different fixed points correspond to different possible patterns in the system.

The applicability of our framework relies on the presence of a low-dimensional unstable manifold. It is bound to be useful only if a small number of modes are unstable. There are other instances of patterning (like Notch-Delta patterns), where many unstable directions exist and the Fourier modes are not the right variables to simplify the dynamics of the system.

Nevertheless, since our framework does not rely on any precise form of the equations, we expect it to be applicable to a very large class of systems. For example, the extension to different geometries would be done in an obvious way by using the eigenfunctions of the Laplacian on the given geometry. Similarly, mechanical systems have been shown to have Turing-like instabilities but the nature of the interactions is not relevant for our framework [34, 35].

We expect our framework to be useful in cases where there are putative Turing patterns alongside time and space resolved expression of a marker. Knowing the details of all of the regulatory or signaling components is not necessary. Since the behavior we are trying to model is determined by the unstable eigenvector, the dynamics of every component will follow the dynamics of this eigenvector. This allows us to drastically reduce the number of parameters required to capture the dynamics. For 3-component networks with one unstable mode, the original equations have 18 parameters, whereas our normal form approximation to the dynamics uses only 4 parameters. Moreover, the number of parameters in reaction-diffusion equations increases with the number of components in the equations, so the 10-component network we study technically has 51 parameters but we need only 3 parameters to approximate the dynamics of any given component.

We also demonstrated how the landscape view of Turing patterns changes in the presence of an external morphogen. Earlier studies had pointed out the difference between field and rate modulation of Turing patterns by external morphogens [36]. Mathematically speaking, the modulation by an external component makes the parameters of the reaction-diffusion equation dependent on space. Some kinds of modulations will leave the base spatial eigenfunctions unperturbed and only change their dynamics as we observe when we introduce a 'field' like variable. Others may change the eigenfunctions themselves as we observe when we change a 'rate' like variable.

We discover that the sequential appearance of SOX9 expression in the context of digit formation can be modeled as a Turing pattern coupled with a wavefront of a morphogen. While analytical results are more difficult to obtain in this case, we find that an 'independent bump' approximation corresponding to spatially localized eigenfunctions allows us to capture the dynamics.

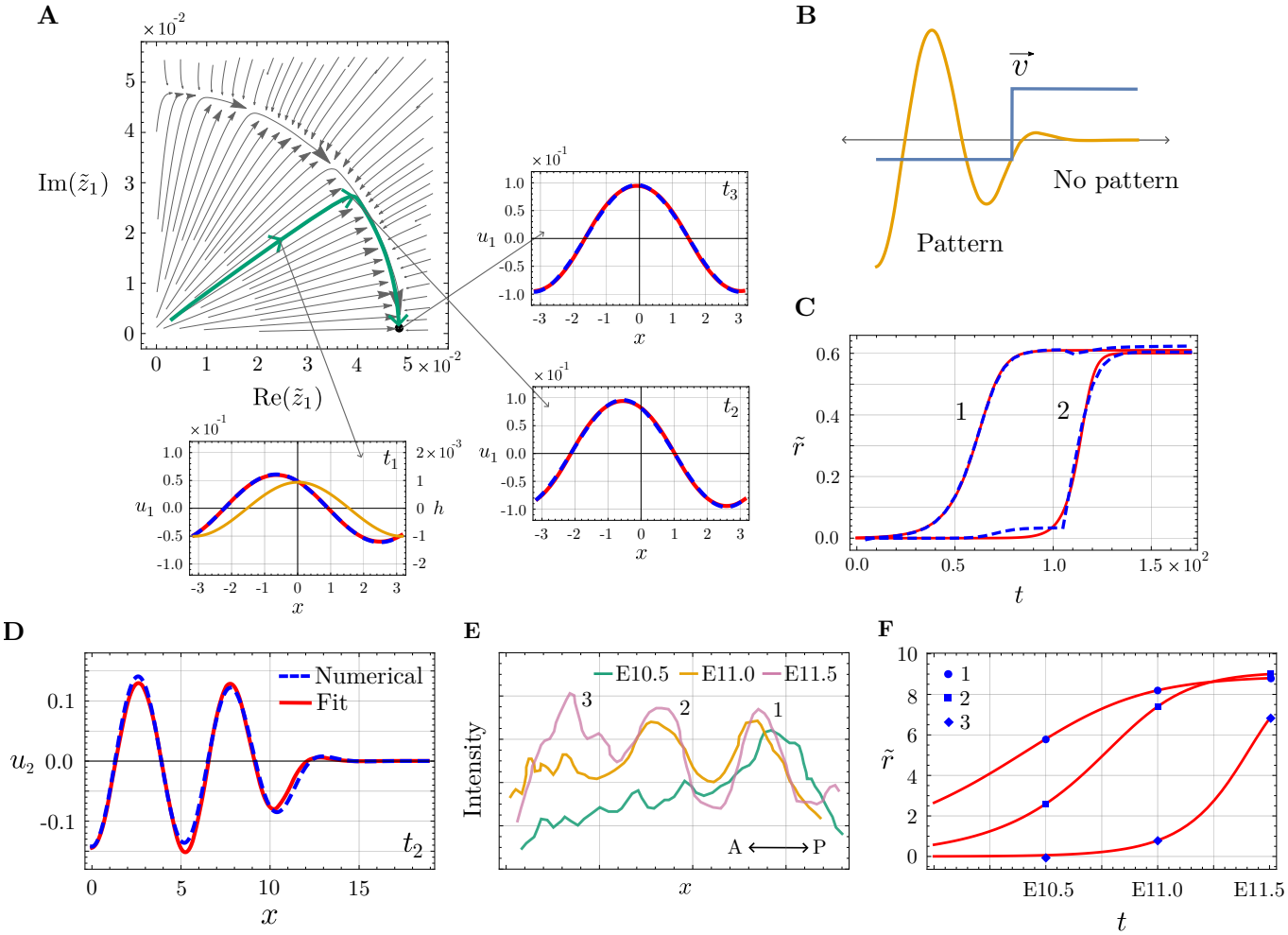

FIG. 5. **Guided organization of Turing patterns with a morphogen gradient and modulated step.** (A) Phase portrait in the $\tilde{z}_1$ plane for a Turing pattern coupled with a small production gradient, which breaks the translational symmetry and leaves only one fixed point determined by the profile of the morphogen gradient. Spatio-temporal dynamics (blue, dashed) and fit to normal form (red) at time $t_1 = 5, t_2 = 20, t_3 = 200$. The pattern eventually aligns with the morphogen gradient. (B) Step modulation in a parameter of the reaction terms takes the dynamics from a non-patterning regime to a patterning regime. (C) The 'independent bump' approximation (see text) fit to the numerical solution. (D) Parameter modulation gives sequential development of pattern (blue, dashed) and fit with the sum of localized eigenfunctions (red) at $t = 120$. (E) Expression of SOX9 along the AP axis at different embryonic time points (data from Fig. 2B in [28]). (F) The 'independent bump' approximation fit (red) with experimental data (blue, points).

The interaction between these modes may lead to much more complex dynamics. Whether such dynamics can be systematically studied will be a topic for future study. Nevertheless, such a systematic investigation will be of value because it will not rely on a particular form of the equations.

One candidate for such a morphogen in the case of digit formation in mice is Shh [37–39]. Shh perturbations lead to successive digital loss which would be consistent with our expectations [40, 41] although the precise role of Shh remains under debate [42–44]. If such a modulating morphogen is quantitatively changed, this would be a powerful use of our framework and its predictions.

There are a few different kinds of perturbations that can be parameterized in our framework. One can shift the center of the dispersion relation and change the most unstable mode. This was suggested to be the role of Hox mutants in digit patterning, although the interpretation of these mutants is disputed [45, 46]. More subtle perturbations may only change the timing of pattern formation, which would be modeled by changes in the parameters that describe the normal form flow [47]. The structure of how these parameters depend on possible perturbations needs to be investigated, but previous studies in the case of cell fate have found that simple linear dependence often captures the dynamics quantitatively [4].

Our framework may also be a natural way to investigate the robustness of Turing patterns. The robustness

of a pattern corresponds to the domain of attraction of its attractor in the landscape. Some studies have suggested that the sequential appearance of patterns may be a more robust way to get a fixed number of patterns [31]. It would be interesting to investigate if this can be shown using our framework.

Our work contributes to the growing theoretical literature on the nonlinear analysis of Turing patterns [48, 49]. However, as mentioned in the Introduction, we distinguish our work from the substantial work on weakly nonlinear analysis of Turing patterns using amplitude equations [22, 50]. While our approach is similar in spirit to Landau-Ginzberg theory, the application of normal form theory gives a distinct prescription on how to quantitatively describe data independent of underlying molecular equations.

Finally, we note that the normal form framework also allows the appearance of fifth-order terms and other resonances in the equations for the modes. While we did not need to include these terms for the cases we investigated, it is possible that such terms may be needed in cases of more complex dynamics like oscillations, which have been observed [51]. Similarly, we expect these terms to be important in the case of subcritical bifurcations.

Ultimately, we believe that our description of Turing patterns will be useful for the study and description of their dynamics in the context of developmental patterns as more quantitative data on gene expression becomes available.

IV. METHODS

Normal form theory

We linearize Equation (1) around the homogeneous fixed point, project along the unstable eigenvector and Taylor expand the nonlinearity. Detailed derivations are given in Section I in the SI. The equations of motion obtained as a result only allow certain terms. In terms of the Fourier modes z_1 and z_2 corresponding to $k = 1$ and $k = 2$ we get

$$\begin{aligned} \dot{z}_1 &= \lambda_1 z_1 - 2\beta_2 z_1^* z_2 - \beta_3 z_1(|z_1|^2 + 2|z_2|^2) + \cdots \\ \dot{z}_2 &= \lambda_2 z_2 - \beta_2 z_1^2 - \beta_3 z_2(|z_2|^2 + 2|z_1|^2) + \cdots \end{aligned} \tag{6}$$

We denote the normal form coordinate corresponding to z_1 by $\tilde{z}_1$. We can remove all non-resonant terms by a change of coordinates (Section II, SI). For one unstable mode $k = 1$, the equations in the normal form coordinates are given by

$$\begin{aligned} \dot{\tilde{z}}_1 &= \lambda_1 \tilde{z}_1 - \beta_3 \tilde{z}_1 |\tilde{z}_1|^2 - \beta_5 \tilde{z}_1 |\tilde{z}_1|^4, \\ \dot{\tilde{z}}_2 &= \lambda_2 \tilde{z}_2 - 2\beta_3 \tilde{z}_2 |\tilde{z}_1|^2 - 3\beta_5 \tilde{z}_2 |\tilde{z}_1|^4. \end{aligned} \tag{7}$$

Note we assume that the bifurcation makes λ_1 positive whereas λ_2 is negative. If the cubic term is stabilizing $\beta_3 > 0$, then we can ignore the β_5 term and only concentrate on the dynamics of the first mode. We next do a perturbation theory where we assume that all other modes remain small in the normal form coordinates (note that this does not imply they remain small in the original coordinates). Hence, to capture the dynamics of the stable modes, we need to find the lowest-order contribution of the unstable mode to their equations. This gives $z_k = c_k(\tilde{z}_1)^k$ for $k \geq 2$ where we have combined the β_k and $(k\lambda_1 - \lambda_k)$ in Equation (3) into one parameter c_k (Section II C, SI). This map is time-independent but allows us to capture the dynamics of modes at any time. Hence, our final approximation to the concentration of any given component is given by Equation (4) with corrections from stable modes. We model the reaction dynamics of the network shown in Fig. 3A with Hill functions and the corresponding reaction-diffusion equations are given by

$$\begin{aligned} \partial_t u_1 &= v_1 H_a[k_{11}] H_r[k_{21}] + \nu_1 - \mu_1 u_1 + d_1 \partial_x^2 u_1, \\ \partial_t u_2 &= v_2 H_a[k_{12}] H_r[k_{32}] + \nu_2 - \mu_2 u_2 + d_2 \partial_x^2 u_2, \\ \partial_t u_3 &= v_3 H_r[k_{13}] H_r[k_{23}] H_a[k_{33}] + \nu_3 - \mu_3 u_3, \end{aligned} \tag{8}$$

where $H_a[k_{ij}] = (1 + (k_{ij}/u_i)^n)^{-1}$ and $H_r[k_{ij}] = (1 + (u_i/k_{ij})^n)^{-1}$ are Hill activation and repression functions respectively. Parameters are given in Section III A in the SI. The dynamics of the component $u_3(x,t)$ is projected along the unstable mode ($k = 1$) and λ_1 and β_3 are obtained from fitting the curve obtained from this projection (Fig 3B). The angle remains constant during the dynamics and the evolution along the radial direction is simply given by $\dot{r} = \lambda_1 r - \beta_3 r^3$. The parameters of the fit have a simple interpretation. The linear growth rate around the instability is given by λ_1 and the pattern saturates at $r_0 = (\lambda_1/\beta_3)^{1/2}$. The angle $\theta = \pi/6$ is determined from the initial condition. We obtain $\lambda_1 = 8.3 \times 10^{-2}, \beta_3 = 6.06 \times 10^{-5}$ for the fit in Fig. 3B. We keep two stable modes with coefficients $c_2 = 7 \times 10^{-3}, c_3 = 2 \times 10^{-5}$ to fit the pattern in Fig. 3C.

The fitting procedure for two unstable modes ($k = 1, 2$) extends the above procedure. In normal form equations, we need to keep both $\tilde{z}_1$ and $\tilde{z}_2$ and with $\theta_1 = \theta_2 = 0$, the radial dynamics is given by

$$\begin{aligned} \dot{r}_1 &= \lambda_1 r_1 - 2\beta_2 r_1 r_2 - \beta_3 r_1 (r_1^2 + 2r_2^2), \\ \dot{r}_2 &= \lambda_2 r_2 - \beta_2 r_1^2 - \beta_3 r_2 (r_2^2 + 2r_1^2). \end{aligned} \tag{9}$$

Parameters used to fit the radial dynamics in Fig. 3D are $\lambda_1 = 9 \times 10^{-2}, \lambda_2 = 4.3 \times 10^{-2}, \beta_2 = -8.5 \times 10^{-4}, \beta_3 = 4.2 \times 10^{-5}$. For the map onto stable modes, we need to keep all the terms involving the two unstable modes. We require one stable mode $k_3 = c_1 \tilde{z}_1^3 + c_2 \tilde{z}_1 \tilde{z}_2$ and parameter values $c_1 = 10^{-5}, c_2 = 10^{-4}$ to fit the pattern in Fig. 3E.

Pattern formation on a 2D domain

The procedure described above can be extended to two spatial directions. To demonstrate this, we solve Equa-

tion (8) on a 2D square domain with parameter values as given in Section III A in the SI. We also keep the diffusion constants in the two directions identical. We denote the mode $e^{i(k_x x+k_y y)}$ with (k_x, k_y). For the given parameters, only the combinations $(k_x, k_y) = (1, 0)$ and $(k_x, k_y) = (0, 1)$ are unstable. We denote the corresponding amplitudes as z_{10} and z_{01}. The normal form dynamics is given by

$$\begin{aligned} \dot{\tilde{z}}_{10} &= \lambda_1 \tilde{z}_{10} - \beta_3(\tilde{z}_{10}|\tilde{z}_{10}|^2 + 2\tilde{z}_{10}|\tilde{z}_{01}|^2), \\ \dot{\tilde{z}}_{01} &= \lambda_1 \tilde{z}_{01} - \beta_3(\tilde{z}_{01}|\tilde{z}_{01}|^2 + 2\tilde{z}_{01}|\tilde{z}_{10}|^2). \end{aligned} \tag{10}$$

For stripe patterns along the x axis, we can ignore $\tilde{z}_{01}$ in the above equations. We look at the dynamics of u_3 along the $y = 0$ axis for the domain $x \in [-\pi, \pi]$ to obtain Fig. 4C. The fitting procedure is the same as done earlier for the 1D domain but we have to keep three stable modes. We use $\lambda_1 = 0.105, \beta_3 = 1.95 \times 10^{-4}$ and coefficients for stable modes $c_1 = 0.024, c_2 = 4.9 \times 10^{-4}, c_3 = 9 \times 10^{-6}$ for the fit in Fig 3B and Fig 3C.

Construction of the Jacobian for a large network

For the dynamics of the network shown in Fig. 4D, we directly construct the Jacobian and saturate the dynamics with a cubic nonlinearity. We construct the Jacobian matrix as $J = G - \eta\mathbb{I}$ where G is a random matrix with elements g_{ij} taken from a Gaussian distribution with zero mean and σ^2 variance. Diagonal terms are set to zero. Without diffusion, we require all the eigenvalues of the Jacobian to be negative. The eigenvalues are distributed in the large N limit according to the circular law and so we can ensure stability by requiring $\eta > \sigma\sqrt{N}$. For $N = 10$ components, we take $\sigma = 0.1, \eta = 2$. With three diffusible components and diffusion constants $d_2 = 0.05, d_4 = 1, d_5 = 2$, we get a positive eigenvalue for the first $(k = 1)$ mode. The Jacobian matrix used is given in Section III B in the SI. For our normal form fit, we look at the dynamics of two components and use $\lambda_1 = 0.039, \beta_3 = 2.91$ for u_2 and $\lambda_1 = 0.039, \beta_3 = 0.36$ for u_8 to fit the dynamics along unstable mode in Fig. 4E. As there are no quadratic terms in the reaction-diffusion equations, we only need one stable component corresponding to $k = 3$ mode in the map to Fourier space. We use $c_3 = -2$ for u_2 and $c_3 = -0.3$ for u_8 to fit the pattern in Fig. 4F.

Pattern alignment with a production gradient

For simplicity, we model a three-component network by directly specifying the Jacobian and using cubic saturation terms. We add a production gradient $h(x)$ in the equation for u_1 and a parameter gradient by modulating the parameter k_{13} as $k_{13}(1 - s(x, t))$.

$$\begin{aligned} \partial_t u_1 &= k_{11}u_1 + k_{31}u_3 - u_1^3 + d_1\partial_x^2 u_1 + h(x), \\ \partial_t u_2 &= k_{22}u_2 + k_{32}u_3 - u_2^3 + d_2\partial_x^2 u_2, \\ \partial_t u_3 &= k_{13}(1 - s(x, t))u_1 + k_{23}u_2 + k_{33}u_3 - u_3^3. \end{aligned} \tag{11}$$

Parameters are given in the Section III C in the SI. First, we investigate the effect of a field $h(x)$ with $s(x, t) = 0$. Since we use periodic boundary conditions, we define the external morphogen gradient to be periodic, $h(x) = p\cos(x)$. The radial dynamics is the same as before, but the angular dynamics is now nontrivial. For one unstable mode, the equations for the radial and angular directions are

$$\begin{aligned} \dot{r} &= \lambda_1 r - \beta_3 r^3 + p\cos(\theta), \\ \dot{\theta} &= -pr^{-1}\sin(\theta). \end{aligned} \tag{12}$$

For small perturbations, we can ignore the $p\cos\theta$ term in the radial part and approximate the radial dynamics as before with $\lambda_1 = 0.49, \beta_3 = 213.14$. Further, assuming a separation of time-scales between the radial and angular dynamics, we can set the value of r to its steady state value $r_0 = \sqrt{\lambda_1/\beta_3}$ in $\dot{\theta}$ equation. The solution is given by $\theta(t) = 2\tan^{-1}\left[c_0 \exp\left(-pr_0^{-1}t\right)\right]$ where c_0 is determined by the initial condition. We use $p = 5.23 \times 10^{-4}$ to fit the angular dynamics in Fig. 5B. The plots for the radial and angular dynamics with the fit are shown in Section III C in the SI.

Sequential patterns

To get the sequential dynamics, we take $s(x, t)$ to be a step function that takes values 0 or 1 and set the field $h(x)$ to zero in Equation (11). The step function effectively changes the parameter value k_{13} and the two values obtained either have stability $(s(x, t) = 1)$ or one unstable mode $(s(x, t) = 0)$, consequently dividing regions into non-patterning and patterning. With $x - 2\pi\lceil t/T\rceil$ as the argument of the step function, from $t = 0$ to $t = T$ pattern forms in $x \in [0, 2\pi]$ and is suppressed for $x > 2\pi$. After $T = 100$ the step function shifts by 2π allowing the pattern to form in $x \in [0, 4\pi]$. In this way we get the bumps to appear one after the other. This is easily extended to get an arbitrary number of bumps that arise in sequential manner.

We fit the dynamics of two bumps to the sum of eigenfunctions $\sum_{i=1,2} r_i(t)\psi_i(x)$. The eigenfunctions $\psi_i(x)$ are calculated numerically with $s(x, t)$ given by a time-independent function $\Theta(\xi_i - x) - \Theta(x - 2\pi - \xi_i)$, where Θ is the Heaviside function and ξ_i is a constant shift. The function takes value 0 on $(\xi_i, 2\pi + \xi_i)$ and 1 elsewhere, ensuring the instability is localized within 2π domain length. The eigenfunctions are calculated subject to no-flux boundary condition. The shift ξ_i is a parameter to be fit and we use $\xi_1 = 0$ and $\xi_2 = 1.63\pi$ to get the two eigenfunctions (Fig. S4, SI). With the 'independent bump' approximation, the dynamics of the amplitudes r_1 and r_2

is taken to follow the radial part of Equation (2). The dynamics is fit to coefficients $c_1(t)$ and $c_2(t)$ obtained by fitting the sum of eigenfunctions to the pattern $u_1(x,t)$ at each timepoint. We employ the same fitting procedure as used for the single unstable mode in Section IV. However, the initial condition has to be treated as a parameter to be fit. We use $\lambda_1 = 0.091, \beta_3 = 0.24, c_0 = 1.3 \times 10^{-3}$ and $\lambda_1 = 0.16, \beta_3 = 0.45, c_0 = 2.66 \times 10^{-9}$ to fit amplitude dynamics of the first and second bumps respectively (Fig. 5C). As the two bumps saturate to the same magnitude, the steady state value $r_0 = \sqrt{\lambda_1/\beta_3}$ is the same for both r_1 and r_2. Hence, we effectively require only two parameters to fit the second bump. With the dynamics described above, the fit to the numerical solution is shown in Fig. 5D.

The data for the dynamics of SOX9 expression (Fig. 5E) along the AP axis is taken from Fig. 2B in Ref. [28]. We remove the mean dynamics from the data (Section III D, SI). The values of the intensity and space are set in arbitrary units to $y \in [0, 10]$ and $x \in [0, 6\pi]$. The fitting follows the same procedure used for the sequential two-bump dynamics. We fit the dynamics of the three bumps to $\sum_{i=1}^{3} r_i(t)\psi_i(x)$. The eigenfunctions are numerically calculated with the same function $s(x,t)$ and we use shift values $\xi_1 = 0.6, \xi_2 = 1.6\pi$, and $\xi_3 = 3.57\pi$. The dynamics of each amplitude, which follows radial part of Equation (2), is fit to coefficients obtained by fitting sum of eigenfunctions to the SOX9 expression data at each timepoint. The normal form fit for the three bumps is shown in Fig. 5F. We use parameters $\lambda_1 = 1.01, \beta_3 = 1.27\times10^{-2}, c_0 = 1.001$ for the first bump, $\lambda_1 = 1.54, \beta_3 = 1.86 \times 10^{-2}, c_0 = 0.12$ for the second bump, and $\lambda_1 = 2.56, \beta_3 = 3.15 \times 10^{-2}, c_0 = 3.57 \times 10^{-4}$ for the third bump.

ACKNOWLEDGEMENTS

We acknowledge support from the Department of Atomic Energy, Government of India (under project RTI4006) and the Simons Foundation (287975). We thank Philip Maini and Tosif Ahamed for their critical reading of a draft of this manuscript and helpful suggestions. SS would like to thank Ankit Dhanuka for helpful discussions.

[1] David A Rand, Archishman Raju, Meritxell Sáez, Francis Corson, and Eric D Siggia. Geometry of gene regulatory dynamics. *Proceedings of the National Academy of Sciences*, 118(38):e2109729118, 2021.

[2] Francis Corson and Eric D Siggia. Gene-free methodology for cell fate dynamics during development. *Elife*, 6:e30743, 2017.

[3] Archishman Raju and Eric D Siggia. A geometrical model of cell fate specification in the mouse blastocyst. *Development*, 151(8), 2024.

[4] Meritxell Sáez, Robert Blassberg, Elena Camacho-Aguilar, Eric D Siggia, David A Rand, and James Briscoe. Statistically derived geometrical landscapes capture principles of decision-making dynamics during cell fate transitions. *Cell Systems*, 13(1):12–28, 2022.

[5] Conrad Hal Waddington. *The Strategy of the Genes*. Routledge, 2014.

[6] Paul François and Eric D Siggia. Phenotypic models of evolution and development: geometry as destiny. *Current Opinion in Genetics & Development*, 22(6):627–633, 2012.

[7] Laurent Jutras-Dubé, Ezzat El-Sherif, and Paul François. Geometric models for robust encoding of dynamical information into embryonic patterns. *Elife*, 9:e55778, 2020.

[8] Francis Corson, Lydie Couturier, Hervé Rouault, Khalil Mazouni, and François Schweisguth. Self-organized Notch dynamics generate stereotyped sensory organ patterns in Drosophila. *Science*, 356(6337):eaai7407, 2017.

[9] A M Turing. The chemical basis of morphogenesis. *Philos. Trans. R. Soc. Lond.*, 237(641):37–72, 1952.

[10] Alfred Gierer and Hans Meinhardt. A theory of biological pattern formation. *Kybernetik*, 12:30–39, 1972.

[11] Akiko Nakamasu, Go Takahashi, Akio Kanbe, and Shigeru Kondo. Interactions between zebrafish pigment cells responsible for the generation of Turing patterns. *Proceedings of the National Academy of Sciences*, 106(21):8429–8434, 2009.

[12] Patrick Müller, Katherine W Rogers, Ben M Jordan, Joon S Lee, Drew Robson, Sharad Ramanathan, and Alexander F Schier. Differential diffusivity of Nodal and Lefty underlies a reaction-diffusion patterning system. *Science*, 336(6082):721–724, 2012.

[13] Takashi Miura and Kohei Shiota. TGFβ2 acts as an "Activator" molecule in reaction-diffusion model and is involved in cell sorting phenomenon in mouse limb micromass culture. *Developmental Dynamics: an official publication of the American Association of Anatomists*, 217(3):241–249, 2000.

[14] Luciano Marcon and James Sharpe. Turing patterns in development: what about the horse part? *Current Opinion in Genetics & Development*, 22(6):578–584, 2012.

[15] Luciano Marcon, Xavier Diego, James Sharpe, and Patrick Müller. High-throughput mathematical analysis identifies Turing networks for patterning with equally diffusing signals. *Elife*, 5:e14022, 2016.

[16] Shigeru Kondo and Takashi Miura. Reaction-diffusion model as a framework for understanding biological pattern formation. *Science*, 329(5999):1616–1620, 2010.

[17] Natalie S Scholes, David Schnoerr, Mark Isalan, and Michael PH Stumpf. A comprehensive network atlas reveals that Turing patterns are common but not robust. *Cell systems*, 9(3):243–257, 2019.

[18] M Mocarlo Zheng, Bin Shao, and Qi Ouyang. Identifying network topologies that can generate turing pattern. *Journal of Theoretical Biology*, 408:88–96, 2016.

[19] Jeremy Green and James Sharpe. Positional information and reaction-diffusion: two big ideas in developmental biology combine. *Development*, 142(7):1203–1211, 2015.

[20] Debbie L Benson, Jonathan A Sherratt, and Philip K Maini. Diffusion driven instability in an inhomogeneous domain. *Bulletin of Mathematical Biology*, 55(2):365–384, 1993.

[21] Tilmann Glimm, Jianying Zhang, and Yun-Qiu Shen. Interaction of Turing patterns with an external linear morphogen gradient. *Nonlinearity*, 22(10):2541, 2009.

[22] Mark C Cross and Pierre C Hohenberg. Pattern formation outside of equilibrium. *Reviews of Modern Physics*, 65(3):851, 1993.

[23] Paul Manneville. *Dissipative Structures and Weak Turbulence*. Springer, 2005.

[24] Yanyan Chen and Javier Buceta. A non-linear analysis of Turing pattern formation. *PloS one*, 14(8):e0220994, 2019.

[25] Thomas E Woolley. Bespoke Turing patterns with specific nonlinear properties. *Proceedings of the Royal Society A*, 481(2312):20250030, 2025.

[26] H Haken and H Olbrich. Analytical treatment of pattern formation in the Gierer-Meinhardt model of morphogenesis. *Journal of Mathematical Biology*, 6:317–331, 1978.

[27] Stephen Wiggins. *Introduction to Applied Nonlinear Dynamical Systems and Chaos*. Springer, 2003.

[28] Jelena Raspopovic, Luciano Marcon, Laura Russo, and James Sharpe. Digit patterning is controlled by a Bmp-Sox9-Wnt Turing network modulated by morphogen gradients. *Science*, 345(6196):566–570, 2014.

[29] Hazlam S Ahmad Shaberi, Aibek Kappassov, Antonio Matas-Gil, and Robert G Endres. Optimal network sizes for most robust Turing patterns. *bioRxiv*, pages 2024–10, 2024.

[30] Vit Piskovsky and Philip K Maini. Will a large complex system form Turing patterns? *bioRxiv*, pages 2024–10, 2024.

[31] Philip K Maini, Thomas E Woolley, Ruth E Baker, Eamonn A Gaffney, and S Seirin Lee. Turing's model for biological pattern formation and the robustness problem. *Interface focus*, 2(4):487–496, 2012.

[32] Edmund J Crampin, Eamonn A Gaffney, and Philip K Maini. Reaction and diffusion on growing domains: scenarios for robust pattern formation. *Bulletin of Mathematical Biology*, 61(6):1093–1120, 1999.

[33] Jake Cornwall Scoones, Deb Sankar Banerjee, and Shiladitya Banerjee. Size-regulated symmetry breaking in reaction-diffusion models of developmental transitions. *Cells*, 9(7):1646, 2020.

[34] Tom W Hiscock and Sean G Megason. Mathematically guided approaches to distinguish models of periodic patterning. *Development*, 142(3):409–419, 2015.

[35] Sifan Yin and L Mahadevan. Contractility-induced phase separation in active solids. *Physical Review Letters*, 131(14):148401, 2023.

[36] Tom W Hiscock and Sean G Megason. Orientation of Turing-like patterns by morphogen gradients and tissue anisotropies. *Cell Systems*, 1(6):408–416, 2015.

[37] Brian D Harfe, Paul J Scherz, Sahar Nissim, Hua Tian, Andrew P McMahon, and Clifford J Tabin. Evidence for an expansion-based temporal Shh gradient in specifying vertebrate digit identities. *Cell*, 118(4):517–528, 2004.

[38] Zsombor Varga and Máté Varga. Gene expression changes during the evolution of the tetrapod limb. *Biologia Futura*, 73(4):411–426, 2022.

[39] Lewis S Mosby, Amy E Bowen, and Zena Hadjivasiliou. Morphogens in the evolution of size, shape and patterning. *Development*, 151(18):dev202412, 2024.

[40] Paul J Scherz, Edwina McGlinn, Sahar Nissim, and Clifford J Tabin. Extended exposure to Sonic hedgehog is required for patterning the posterior digits of the vertebrate limb. *Developmental Biology*, 308(2):343–354, 2007.

[41] Jianjian Zhu, Eiichiro Nakamura, Minh-Thanh Nguyen, Xiaozhong Bao, Haruhiko Akiyama, and Susan Mackem. Uncoupling Sonic hedgehog control of pattern and expansion of the developing limb bud. *Developmental cell*, 14(4):624–632, 2008.

[42] Meng Zhu and Clifford J Tabin. The role of timing in the development and evolution of the limb. *Frontiers in Cell and Developmental Biology*, 11:1135519, 2023.

[43] Jianjian Zhu, Rashmi Patel, Anna Trofka, Brian D Harfe, and Susan Mackem. Sonic hedgehog is not a limb morphogen but acts as a trigger to specify all digits in mice. *Developmental Cell*, 57(17):2048–2062, 2022.

[44] Rushikesh Sheth, Damien Grégoire, Annie Dumouchel, Martina Scotti, Jessica My Trang Pham, Stephen Nemec, Maria Félix Bastida, Marian A Ros, and Marie Kmita. Decoupling the function of Hox and Shh in developing limb reveals multiple inputs of Hox genes on limb growth. *Development*, 140(10):2130–2138, 2013.

[45] Rushikesh Sheth, Luciano Marcon, M Félix Bastida, Marisa Junco, Laura Quintana, Randall Dahn, Marie Kmita, James Sharpe, and Maria A Ros. Hox genes regulate digit patterning by controlling the wavelength of a Turing-type mechanism. *Science*, 338(6113):1476–1480, 2012.

[46] Tom W Hiscock, Patrick Tschopp, and Clifford J Tabin. On the formation of digits and joints during limb development. *Developmental cell*, 41(5):459–465, 2017.

[47] Takashi Miura and Philip K Maini. Speed of pattern appearance in reaction-diffusion models: implications in the pattern formation of limb bud mesenchyme cells. *Bulletin of Mathematical Biology*, 66(4):627–649, 2004.

[48] Robert A Van Gorder. Pattern formation from spatially heterogeneous reaction–diffusion systems. *Philosophical Transactions of the Royal Society A*, 379(2213):20210001, 2021.

[49] Andrew L Krause, Eamonn A Gaffney, Philip K Maini, and Václav Klika. Modern perspectives on near-equilibrium analysis of Turing systems. *Philosophical Transactions of the Royal Society A*, 379(2213):20200268, 2021.

[50] Rebecca B Hoyle. *Pattern Formation: An Introduction to Methods*. Cambridge University Press, 2006.

[51] Ryosuke Nishide and Shuji Ishihara. Oscillatory and chaotic pattern dynamics driven by surface curvature. *Physical Review E*, 111(2):L022202, 2025.